Computers in Biology and Medicine 95 (2018) 55–62

Contents lists available at ScienceDirect

Computers in Biology and Medicine

journal homepage: www.elsevier.com/locate/compbiomed

Optimized multi-level elongated quinary patterns for the assessment of thyroid nodules in ultrasound images

U. Raghavendra [a,*], Anjan Gudigar [a], M. Maithri [b], Arkadiusz Gertych [c], Kristen M. Meiburger [d], Chai Hong Yeong [e], Chakri Madla [f], Pailin Kongmebhol [f], Filippo Molinari [d], Kwan Hoong Ng [e], U. Rajendra Acharya [g,h,i]

[a] Department of Instrumentation and Control Engineering, Manipal Institute of Technology, Manipal Academy of Higher Education, Manipal, 576104, India
[b] Department of Mechatronics Engineering, Manipal Institute of Technology, Manipal Academy of Higher Education, Manipal, 576104, India
[c] Department of Surgery, Department of Pathology and Laboratory Medicine, Cedars-Sinai Medical Center, Los Angeles, CA, USA
[d] Department of Electronics and Telecommunications, Politecnico di Torino, Italy
[e] Department of Biomedical Imaging, University of Malaya, Kuala Lumpur, Malaysia
[f] Department of Radiology, Faculty of Medicine, Chiang Mai University, Chiang Mai, 50200, Thailand
[g] Department of Electronics and Computer Engineering, Ngee Ann Polytechnic, Clementi, 599489, Singapore
[h] Department of Biomedical Engineering, School of Science and Technology, SIM University, Clementi, 599491, Singapore
[i] Department of Biomedical Engineering, Faculty of Engineering, University of Malaya, Kuala Lumpur, 50603, Malaysia

ARTICLE INFO

Keywords:
Elongated quinary patterns
Higher order spectra
Particle swarm optimization
Support vector machine
Thyroid cancer
Ultrasound

ABSTRACT

Ultrasound imaging is one of the most common visualizing tools used by radiologists to identify the location of thyroid nodules. However, visual assessment of nodules is difficult and often affected by inter- and intra-observer variabilities. Thus, a computer-aided diagnosis (CAD) system can be helpful to cross-verify the severity of nodules. This paper proposes a new CAD system to characterize thyroid nodules using optimized multi-level elongated quinary patterns. In this study, higher order spectral (HOS) entropy features extracted from these patterns appropriately distinguished benign and malignant nodules under particle swarm optimization (PSO) and support vector machine (SVM) frameworks. Our CAD algorithm achieved a maximum accuracy of 97.71% and 97.01% in private and public datasets respectively. The evaluation of this CAD system on both private and public datasets confirmed its effectiveness as a secondary tool in assisting radiological findings.

1. Introduction

Thyroid cancer is more commonly seen in women compared to men, with the morbidity rate >5% increasing every year [1]. It is estimated that approximately 56,870 new thyroid cancer cases will be diagnosed in 2017 in the United States [2]. The thyroid gland secretes thyroxine (T4) and tri-iodothyronine (T3) hormones that are important for the overall wellbeing of the human body. They mainly regulate metabolism, growth, development, and temperature of the body. They also play a vital role in the development of the brain [3,4].

The enlargement of the thyroid gland is termed goiter. Goiters can be either diffuse, i.e., covering the entire gland, or nodular. These thyroid gland "bumps" are referred to as thyroid nodules [5], and can be either benign or malignant. Early diagnosis improves stratification of thyroid nodules and helps in determining the best treatment option [6].

Ultrasound is an inexpensive and effective method in thyroid imaging. Images of the organs are obtained by capturing echoes which are generated as a response to the sound waves sent from a transducer at a high frequency rate. By analyzing the reflected echoes, it is possible to differentiate healthy and malignant tissues. The ultrasound features of a malignant thyroid nodule include hypoechoic, ill-defined margins and punctate calcification [7]. Ultrasounds also provide a useful tool for disease follow-up in patients with thyroid cancer after treatment.

Thyroid cancer has different stages based on the tumor classification without any definitive demarcation between each stage [8]. The "stage" of a cancer indicates a particular specified level during the tumor growth. Further, computer-aided diagnosis (CAD) of ultrasound images can help the radiologists in early diagnosis of thyroid nodules. The CAD systems often consist of feature extraction and machine learning algorithms. To date, several CADs for thyroid nodule differentiation have been proposed

* Corresponding author. Department of Instrumentation and Control Engineering, Manipal Institute of Technology, Manipal Academy of Higher Education, Manipal, 576104, India.
E-mail address: raghavendra.u@manipal.edu (U. Raghavendra).

https://doi.org/10.1016/j.compbiomed.2018.02.002
Received 13 November 2017; Received in revised form 2 February 2018; Accepted 2 February 2018

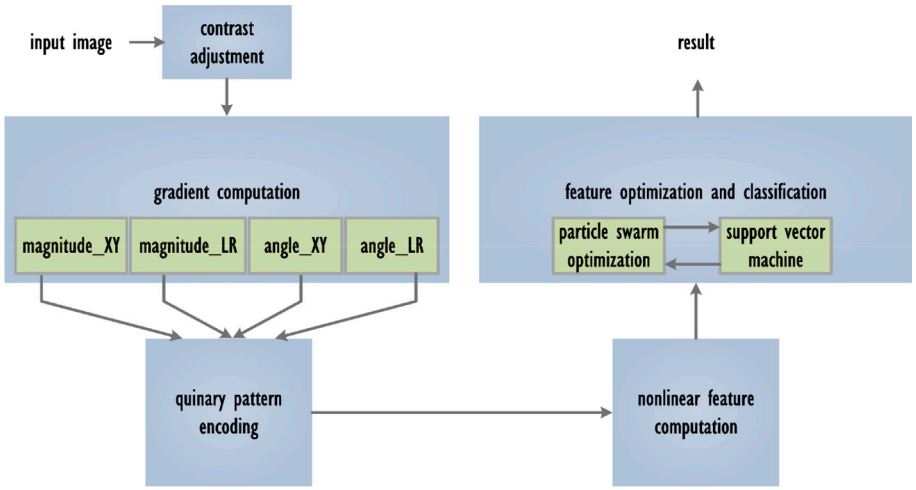

Fig. 1. Overview of the proposed model.

[9–11]. A neural network model described in Ref. [12] has gained an accuracy of 88.3%. In Ref. [13] an accuracy of 81% is achieved using artificial immune recognition system (AIRS). Directionality patterns implemented in Ref. [14] achieved classification accuracy of 89.4%. A neuro-fuzzy classifier proposed in Ref. [15] has shown 95.33% accuracy in diagnosing thyroid lesions. Erol et al. [6] concluded in their experiment that, radial basis function neural network (RBFNN) is a suitable classifier for thyroid disease compared to multilayer perceptron neural network (MLPNN). An information gain based artificial immune recognition system (IG-AIRS) trained on a dataset with thyroid diseases in Ref. [16] yielded an accuracy of 95.90%. A system developed by Dogantekin et al. [17] used principal component analysis (PCA) and SVM and obtained 97.67% accuracy. The discriminant analysis, wavelet features and SVM were used to obtain 91.86% classification accuracy [18].

The parameters of SVM classifier were optimized using particle swarm optimization (PSO), and an average accuracy of 97.49% was attained in Ref. [19]. PCA was used with an extreme learning machine classifier to obtain new feature space for thyroid diseases and achieved a mean accuracy of 97.73%. By adaptively tweaking the parameters for fuzzy k-nearest neighbor (FKNN) classifier, the authors of [20] attained a mean accuracy of 98.82%. Various soft and hard fuzzy clustering techniques used for the thyroid disease classification can be found in Ref. [21].

A texture feature based technique was developed in Ref. [22] and attained a maximum accuracy of 100%. In Ref. [23], a new system is developed using combination of discrete wavelet transform (DWT) and texture features with an AdaBoost classifier for the classification of thyroid lesions. A classification accuracy, sensitivity and specificity of 100% were reported by them. Good classification accuracy was shown by grayscale features based on Gabor wavelet, moments, entropy, image texture and higher order spectra (HOS) features [24]. In a work by Acharya et al. [25] to evaluate Hashimoto thyroiditis, a stationary wavelet transform with fuzzy classifier was used and attained a maximum accuracy, sensitivity, specificity of 84.6%, 82.8%, and 87.0% respectively. In Ref. [26], Gabor transform features with locality sensitive discriminant analysis (LSDA) and C4.5 decision tree classifier were used to classify thyroid nodules, and attained 94.3% accuracy.

In Ref. [27], linear discriminant analysis classifier was used to diagnose Hashimoto's thyroiditis and obtained 96.88% sensitivity, 98.44% specificity, and 97.66% overall classification accuracy. Another system was proposed by Ref. [28], which involved a fine-tuned deep convolutional neural network and pre-processed ultrasound images. This system reported 98.29% accuracy, 99.10% of sensitivity and 93.90% specificity using open access database. And obtained 96.34% accuracy, 86% sensitivity, and 99% specificity with non-public database. In Ref. [29], an artificial neural network (ANN) was applied to detect thyroid nodules in ultrasound images and obtained 70% accuracy. A more advanced system proposed in Ref. [30] utilized a watershed algorithm for the segmentation of nodules and ANN and SVM classifiers for the classification of benign and malignant nodules. The accuracy, specificity, sensitivity and AUC (area under the curve) were 92.5%, 96.66%, 80%, and 0.91 for SVM and 87.5%, 93.33%, 70% and 0.88 for ANN respectively. The authors of this study concluded that the SVM classifier is more stable and reliable compared to the ANN classifier. In a study involving extraction and classification of elastography features from ultrasound images of thyroid nodules [31], an LDA classifier was used. This was developed to differentiate the thyroid nodules into two types (i) no FNA (fine-needle aspiration) (observation-only) and (ii) FNA. They showed 100% sensitivity and specificity of 75.6% in detecting malignant thyroid nodules. A convolutional neural network model was used to extract the deep features from ultrasound images in Ref. [32] and achieved 92.9% accuracy in the classification of thyroid nodules. An automated CAD system proposed in Ref. [33] used a speckle reduction technique to find and segment a region containing suspicious nodules. This segmentation system achieved true positive of $95.92 \pm 3.70\%$, false positive of $7.04 \pm 4.21\%$, dice coefficient of $93.88 \pm 2.59\%$ and overlap metric of 91.18 ± 7.04 pixels and Hausdorff distance of 0.52 ± 0.20 pixels. Performances of different techniques are presented in Table 5.

However, it is difficult to compare the effectiveness of these techniques because each method used different number of subjects. Ideally, the techniques should be tested using large datasets for confirming their effectiveness. Hence, in this work we have developed a new methodology for the characterization of thyroid lesions using optimized HOS entropies extracted from elongated quinary patterns of multi-level gradients. Our system containing PSO and SVM is developed using private (288 benign, and 56 malignant) and public (288 benign and 57 malignant) datasets. An overview of the proposed model is shown in Fig. 1.

2. Materials and methods

2.1. Data descriptions

In this work, we have used two datasets, one public dataset and another from our own (private) dataset.

Dataset 1 (Public database): Images were taken from an open-access thyroid ultrasound-image database [34] which consists of ultrasound images with thyroid nodules. From this publicly available database, 288 benign and 57 malignant images belong to 99 controls and 200 cases were chosen with age range of $57{:}35 \pm 16{:}2$ years. The ultrasound image sequences were captured with TOSHIBA Nemio 30 and TOSHIBA Nemio MX ultrasound systems, both set to 12 MHz convex and then from this sequence, thyroid images were extracted. The patients were

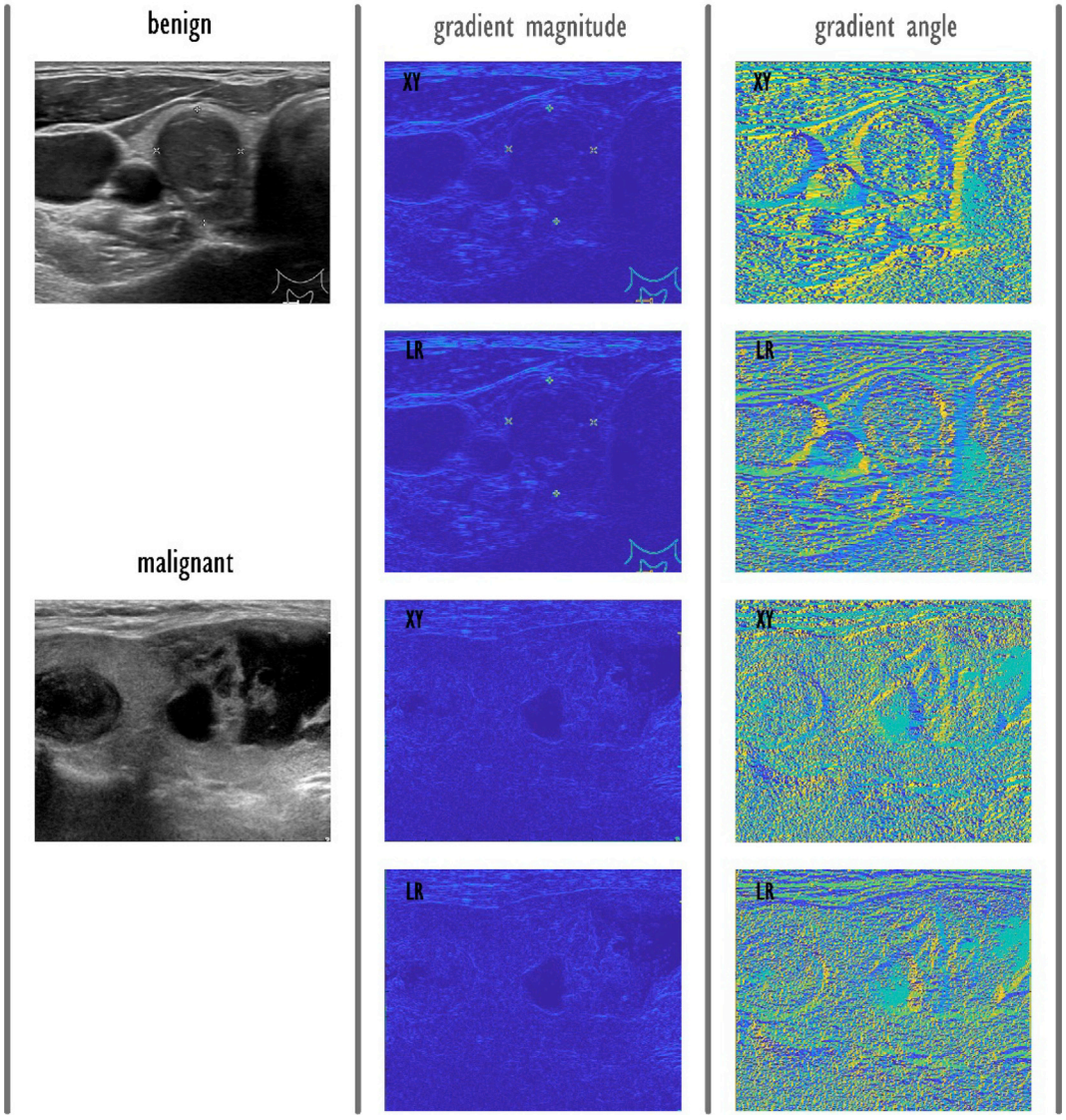

Fig. 2. Magnitude and angle in XY and LR directions.

individually evaluated by two experts and the TI-RAD lexicon description was provided.

Dataset 2 (Private database): This dataset was collected at Chiang Mai University Hospital between December 1st, 2009 and December 31st, 2016. Cytology (by fine needle aspiration biopsy) or surgical excision were used to confirm the presence of benign or malignant nodules. In this study, 344 thyroid nodule images were collected, out of which 288 were benign, and 56 were malignant. The images were collected from patients between 12 and 88 years of age (mean age: 44.1 years). The patients were examined using one of the following scanners: GE LOGIQ 9 and LOGIQ E9 with linear transducer 10–14 MHz, SIEMENS Acuson Sequoia 512 with linear transducer 5–13 MHz, TOSHIBA Aplio-XG with linear transducer 10–13 MHz and PHILIPS iU22 with linear transducer 5–15 MHz, depending on scanner availability. B-Mode images were collected during the examination.

2.2. Feature representation using quinary encoding

Gradients are the effective and robust feature representation techniques used for image analysis [35,36]. Multi-gradient magnitudes and angles are derived from a given image in XY and left-right (LR) directions. To extract gradient components, *four* different Sobel masks were used in various orientations, and the resultant images were used to compute the magnitude and angle of the gradient.

To obtain the gradient in the XY direction, pixels around the center pixel P_{x5} of a sub image of size 3×3 are convolved with the horizontal (H_m) and vertical (V_m) Sobel masks.

$$Gr\_x(H) = (P_{x1} + 2P_{x2} + P_{x3}) - (P_{x7} + 2P_{x8} + P_{x9}) \quad (1)$$

where, the $Gr\_x(H)$ represents the horizontal direction gradient of pixel P_{x5}.

Similarly, the gradient of pixel P_{x5} in vertical direction is given by:

$$Gr\_y(V) = (P_{x1} + 2P_{x4} + P_{x7}) - (P_{x3} + 2P_{x6} + P_{x9}) \quad (2)$$

Using the $Gr\_x(H)$ and $Gr_y(V)$components, the magnitude gradient $Gmag\_xy$ and angle gradient $Gdir\_xy$ are computed. Magnitude gradient is given by

$$Gmag\_xy = |Gr\_x(H)| + |Gr\_y(V)| \quad (3)$$

And angle gradient is

$$Gdir\_xy = \tan^{-1}\left(Gr\_y(V)/Gr\_x(H)\right) \quad (4)$$

Likewise, to obtain the magnitude and angle gradients for the center

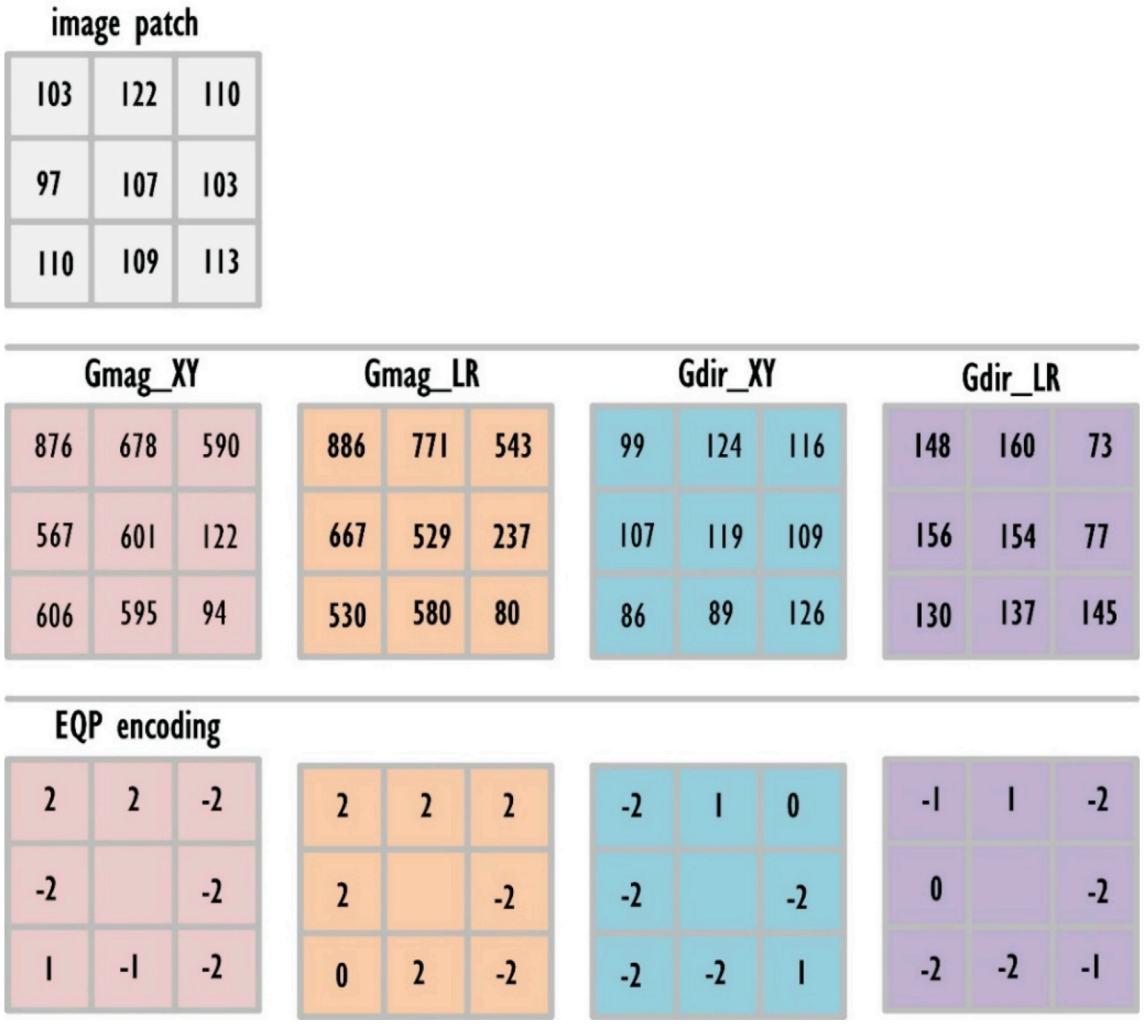

Fig. 3. Example of elongated quinary pattern descriptor.

pixel P_{x5} in L-R direction the center pixel is convolved with the diagonal masks d_1 and d_2. The gradient of the pixel P_{x5} left (l) and right (r) is given by:

$$Gr\_l(d2) = (P_{x2} + 2P_{x3} + P_{x6}) - (P_{x4} + 2P_{x7} + P_{x8}) \quad (5)$$

and

$$Gr\_r(d1) = (P_{x6} + 2P_{x9} + P_{x8}) - (2P_{x1} + P_{x2} + P_{x4}) \quad (6)$$

Using these convolution outputs, magnitude gradient *Gmag_LR* and angle gradient *Gdir_LR* are obtained as follows:

$$Gmag\_LR = |Gr\_l(d2)| + |Gr\_r(d1)| \quad (7)$$

$$Gdir\_LR = \tan^{-1}\left(Gr\_r(d1)/Gr\_l(d2)\right) \quad (8)$$

Fig. 2 shows extracted gradient magnitude and angle in both XY and LR directions.

Regions which have rough versus smooth textures can be isolated using gradient feature extraction technique. The magnitude gradient features are stable and consistent in the edge and curve regions of the images with rough textures. Hence, it becomes easier to isolate regions with the higher intensity regions. The angle gradient features explore the minute features such as bump or swelling at different angles.

The LR and XY gradient magnitudes and angles (eight gradient components) are quantized with an elongated quinary pattern (EQP) technique and *five* levels of encoding [36]. To encode the eight-connected pixel neighborhood, two threshold values Th_1 and Th_2, are used. Various combinations of values were used for Th_1 and Th_2 ranging from 1 to 20 and the performance was observed. The values 4 and 9 for Th_1 and Th_2 respectively showed the highest performance.

The five-level encoding in terms of gradient magnitude as:

$$Gr_{magEQP}(Gr\_mag_p, Gr\_mag_c): \begin{cases} +2 & Gr\_mag_p \geq Gr\_mag_c + Th2 \\ +1 & Gr\_mag_c + Th1 \leq Gr\_mag_p < Gr\_mag_c + Th2 \\ 0 & Gr\_mag_c - Th1 \leq Gr\_mag_p < Gr\_mag_c + Th1 \\ -1 & Gr\_mag_c - Th2 \leq Gr\_mag_p < Gr\_mag_c - Th1 \\ -2 & otherwise \end{cases}$$

where Gr_mag_p signifies the gradient magnitudes of neighboring points which are surrounding this center pixel gradient magnitude (Gr_mag_c).

Fig. 3 shows an example of encoded quinary patterns of magnitude and angle in both the XY and LR direction. Fig. 4 shows the EQP of benign and malignant classes.

2.3. Higher order spectral entropies

Higher order spectra (HOS) is designed for the better spectral representation of stochastic or deterministic processes. It is very useful in the identification of non-linearity in deterministic signals and random processes [37–39]. It has been widely used in medical image analysis [40,], traffic sign recognition [41], and signal analysis [42–44]. Generally, a bispectrum of 2-D signals can be characterized in 4-D. The HOS analysis is a 1-D projection of an image performed at an angle θ using the Radon transform (RT). The bispectrum first, second, third order entropies and also phase entropies are extracted as defined in Refs. [40,45,46] after RT.

Finally, adaptive synthetic (ADASYN) sampling is used to overcome the problem of imbalance in the number of samples between the two classes. It uses the density distribution to govern the number of samples required for the class of minimum samples. The resultant balanced samples with features can be used for further processing [47].

2.4. Feature selection and classification

PSO is a population-based search method which will mimic the flocking behavior of birds and fish swarms [48]. In PSO, the positions of every particle of a given swarm (i.e., population) is updated based on the previous experiences. After the update, new fitness values of these particles are calculated. This process continues until stopping criteria is met. PSO was used to select 5, 10, 15, 20, and 25 top features that were fed to an SVM classifier [49,50], as it has the capacity to generalize by optimizing the margin [51]. The classifier performance was tested with 1st, 2nd and 3rd polynomial, and radial basis function (RBF) kernels to find the best performing classifier. We have considered accuracy, sensitivity and specificity as our performance evaluation metrics.

3. Experimental results

In this study, we have used both public (Benign: 288, Malignant: 57) and private (Benign: 288, Malignant: 56) ultrasound thyroid datasets to

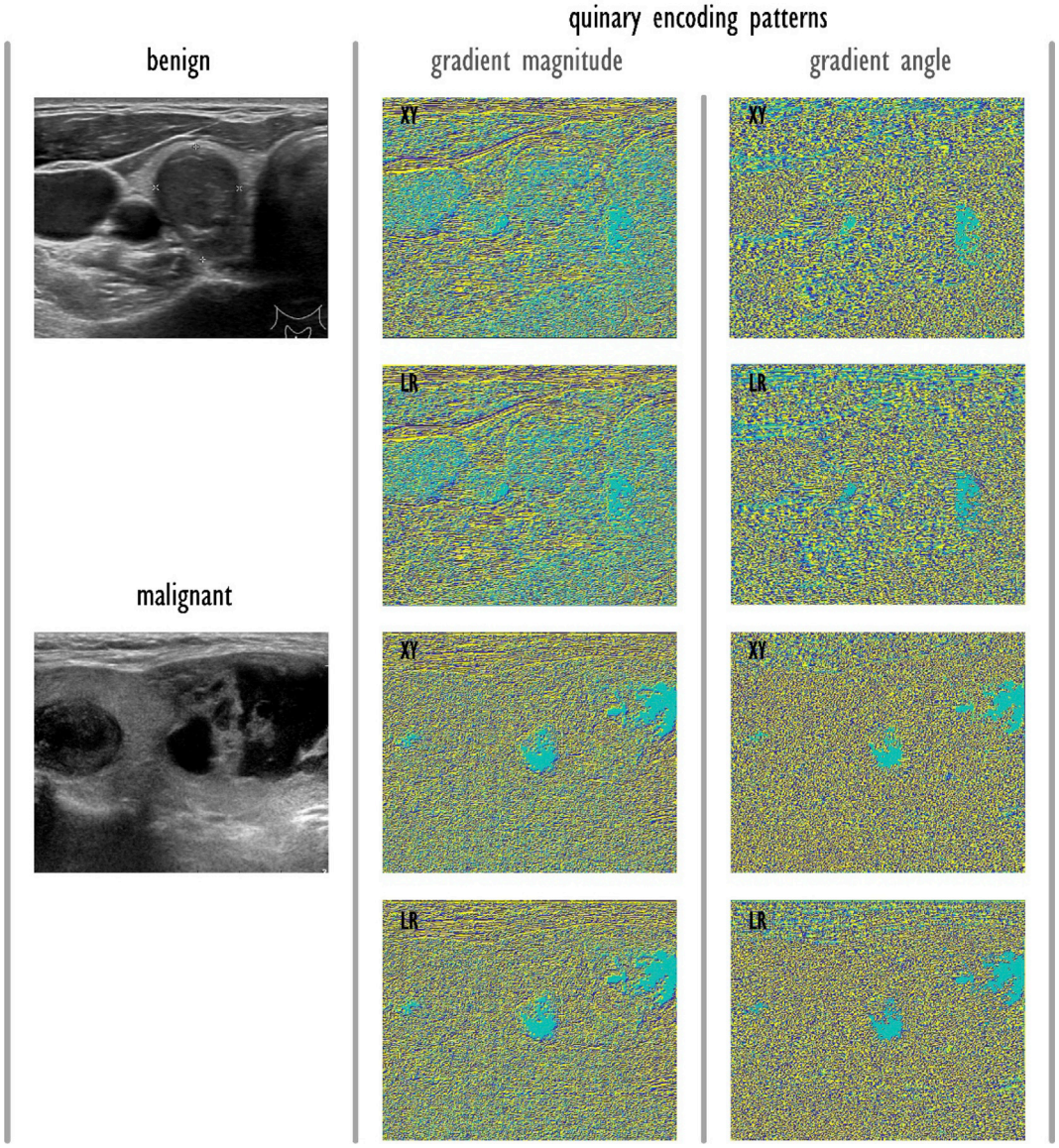

Fig. 4. Elongated quinary patterns of magnitude and angle gradients for example benign and malignant nodules.

develop, and assess the performance of thyroid nodule differentiation. The processing begins with the calculation of multi-level gradient magnitudes and angles in the XY-direction and LR-direction, and yielded *four* different gradient components. Each gradient component is encoded using quinary encoding patterns and their corresponding *seventy two* HOS entropies are extracted ($72 \times 4 = 288$ features). In order to overcome the imbalance in the number of benign and malignant class images, the ADASYN is used. It has created *two hundred twenty four* additional synthetic minority data samples for public as well as private datasets. These features are subjected to PSO to select the most significant features for classification. We have used SVM classifier with different kernel functions for classification. Ten-fold cross validation is used to evaluate the performance of the developed system.

We have performed our experiments by selecting 5, 10, 15, 20 and 25 significant features with various iterations which randomly selects different features using PSO and SVM. The significant features are further tested using 10-fold cross validation. The obtained classification performances for different kernel functions are given in Tables 1 and 2. We have achieved an average performance of 93.89% accuracy, 88.85% sensitivity and 94.66% specificity with *ten* features and *fifteen* iterations using public dataset. We have also achieved an average performance of 91.91% accuracy, 92.85% sensitivity and 88.54% specificity with *ten* features and *twenty* iterations for private dataset. In order to test the usefulness of quinary patterns, we have extracted HOS entropies directly from multi-level gradients and fed to PSO-SVM combination for classification. The obtained results are presented in Tables 3 and 4 for public and private datasets respectively. The average accuracy of 89.92% is achieved with *ten* significant features and *twenty* iterations using the public dataset. It can be observed that the model performed better when HOS entropies are extracted from quinary patterns rather than from gradients. Figs. 5 and 6 shows the performance of the proposed model for different combinations of features and iterations for both public and private datasets.

Table 1
Performance of proposed model for different kernels for public dataset.

SVM Kernel	Iterations	Features	Accuracy (%)	Sensitivity (%)	Specificity (%)
Poly 1	15	10	65.55	61.67	69.75
Poly 2	15	10	76.62	64.45	89.32
Poly 3	15	10	77.50	60.27	95.37
RBF	**15**	**10**	**93.89**	**88.85**	**94.66**

Table 2
Performance of proposed model for different kernels for private dataset.

SVM Kernel	Iterations	Features	Accuracy (%)	Sensitivity (%)	Specificity (%)
Poly 1	20	10	59.15	60.71	57.63
Poly 2	20	10	70.59	81.42	60.06
Poly 3	20	10	80.28	93.92	67.01
RBF	**20**	**10**	**91.91**	**92.85**	**88.54**

Table 3
Performance of HOS entropy extracted from multi-level gradient for different kernels using the public dataset.

SVM Kernel	Iterations	Features	Accuracy (%)	Sensitivity (%)	Specificity (%)
Poly 1	20	10	56.82	57.14	60.14
Poly 2	20	10	69.96	64.80	79.71
Poly 3	20	10	72.18	56.09	93.23
RBF	**20**	**10**	**89.92**	**82.57**	**90.39**

Table 4
Performance of HOS entropy extracted from multi-level gradient for different kernels using private dataset.

SVM Kernel	Iterations	Features	Accuracy (%)	Sensitivity (%)	Specificity (%)
Poly 1	15	10	60.51	60.60	60.41
Poly 2	15	10	71.79	79.46	63.88
Poly 3	15	10	80.17	95.95	63.88
RBF	**15**	**10**	**91.78**	**92.25**	**85.06**

4. Discussion

Ultrasound is the most commonly used modality for the detection and assessment of thyroid nodules. In this study, we have presented a novel

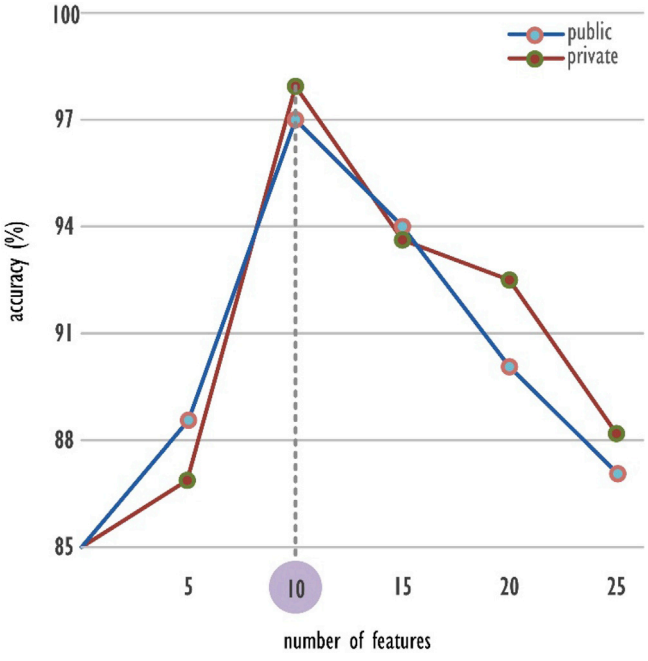

Fig. 5. Performance of the proposed model for change in features with fixed iteration of 10.

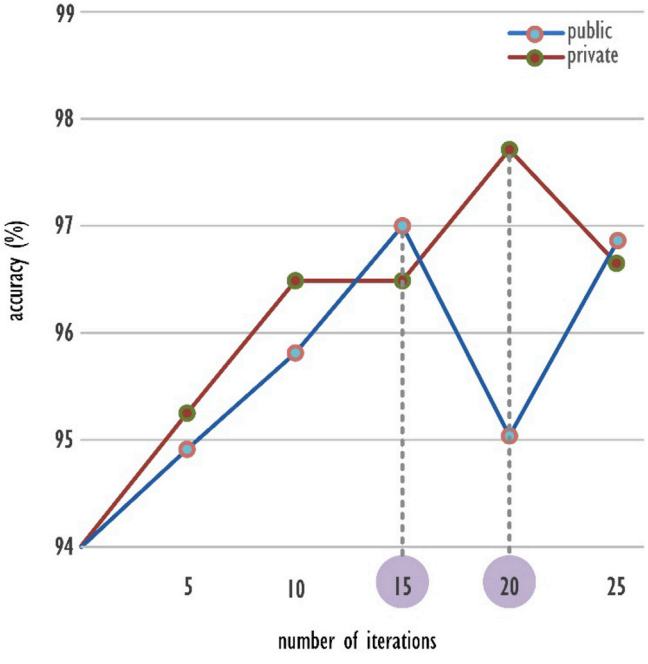

Fig. 6. Performance of the proposed model for change in iteration with fixed features of 10.

Table 5
State-of-the-art techniques for the characterization of thyroid lesions.

Papers	No. of Subjects	Method/Classifier	Accuracy (%)
[12]	215	MLP + RBF + CSFNN	88.3, 81.69 and 85.92
[52]	66	Radon Transform + SVM	89.4
[13]	215	AIRS	81
[14]	66	Radon Transform + SVM	89.4
[15]	215	Neuro Fuzzy classifier	95.33
[16]	215	IG-AIRS	95.90
[53]	85	Morphological + Wavelet features + SVM	AUC: 0.96
[17]	215	PCA + SVM	97.67
[54]	98	k-means clustering + PCA + SVM	87.8
[55]	61	Texture features + SVM	100
[56]	200	Fuzzy local binary patterns + fuzzy grey-level histogram features + SVM	97.5
[18]	215	Discriminant Analysis + Wavelet + Support Vector Machine	91.86
[19]	215	PSO + SVM	97.49
[20]	215	Fuzzy k-nearest neighbor	98.82
[57]	125	Hard area ratio + textural features + SVM	93.6
[58]	142	Textural + shape feature vectors + SVM	AUC: 0.93
[59]	13	GLCM + SVM	84.62
[60]	118	Noise resilient features + SVM	95.2
[22]	10	Texture Feature + SVM	100
[23]	10	DWT + texture + AdaBoost	100
[26]	242	Gabor transform + LSDA + C4.5 decision tree classifier	94.3
[61]	242	Fractal + SGLDF + MFA	97.52
This work	**Public: 345, Private: 344**	**EQP + HOS Entropy + PSO + SVM**	**Private: 97.71, Public: 97.01**

methodology for the characterization of thyroid nodules that belong to either benign or malignant group. We have used encoded quinary patterns of magnitude and angle gradients in two different directions to extract the features and classify the nodules. The gradient magnitudes are efficient in characterizing the textures or regions, whereas angle magnitudes explore minute features such as bumps or swelling [36]. The enhanced gradients are systematically encoded using elongated quinary patterns which automatically reduce the gradient sensitivity by quantizing and encoding in the key regions of thyroid images. The obtained entropy features from these patterns can discriminate benign and malignant lesions during the classification. In addition, the ADASYN synthetic sample generation algorithm helps to compensate the issue of data unbalancing and helps to prevent the over-fitting of classifiers. The extracted features with synthetic samples are fed to the PSO algorithm to select these best features. These selected features were used to train the SVM classifier. Our system required only *ten* significant features from the extracted 288 features to attain 93.89% average accuracy. In order to test the robustness of our model, we have also repeated our experiment using public database and different kernel functions. It is observed that the SVM with RBF kernel has attained maximum performance in all combinations as shown in Tables 1 and 2 We have also observed the superiority of extracting HOS features from EQP patterns than extracting it from multi-level gradients as shown in Tables 3 and 4 as it compensates the gradient sensitivity [36]. Overall performance is boosted approximately by 4% for public dataset. Figs. 5 and 6 yielded the maximum results using combination of PSO and SVM. Our proposed system attained maximum accuracy of 97.71% and 97.01% for private and public datasets respectively. The major observation during our experiment is that, the performance of the developed model is consistent for both public and private datasets irrespective of using the imbalanced data (benign patients are more than malignant) in both cases. Our study used images from public and private repositories and compared with other studies published to date on this topic (Table 5).

5. Conclusion

In this paper, a novel automated CAD system is proposed to characterize thyroid nodules. Our CAD achieved 97.71% maximum accuracy using only *ten* features. The HOS entropies extracted from multi-level elongated quinary patterns delineate the non-linearity among benign and malignant classes thereby providing the best discrimination of nodules. The PSO-SVM framework helped to select the most significant features, and achieve maximum performance with minimum features. The developed system is robust as it yielded the highest performance for both private and public datasets with the same number of features. This CAD can be used as a screening tool to assist the clinicians during their routine checkups for thyroid nodules.

Conflicts of interest

We hereby confirm that none of the authors have any conflict of interest related to this manuscript.

References

[1] K.D. Miller, R.L. Siegel, C.C. Lin, et al., Cancer treatment and survivorship statistics, 2016, CA Cancer J Clin. 66 (2016) 271–289.
[2] National Cancer Institute, https://seer.cancer.gov/statfacts/html/thyro.html (Last Accessed: 13.05.2017).
[3] H.J. Biersack, F. Grünwald, Thyroid Cancer, second ed., Springer, Berlin, 2005.
[4] https://www.quora.com/Why-is-Thyroxine-called-the-personality-hormone] (Last accessed: 30.10.2017).
[5] https://www.cancer.org/cancer/thyroid-cancer/about/what-is-thyroid-cancer.html] (Last accessed: 30.10.2017).
[6] R. Erol, S.N. Ogulata, C. Sahin, Z.N. Alparslan, A radial basis function neural network (rbfnn) approach for structural classification of thyroid diseases, J. Med. Syst. 32 (3) (2008) 215–220.
[7] K.T. Wong, Anil T. Ahuja, Ultrasound of thyroid cancer, Canc. Imag. 5 (1) (2005) 157–166.
[8] L. Wartofsky, Staging of thyroid cancer, in: L. Wartofsky, D. Van Nostrand (Eds.), Thyroid Cancer, Springer, New York, NY, 2016.
[9] U.R. Acharya, G. Swapna, S. Vinitha Sree, F. Molinari, S. Gupta, R.H. Bardales, A. Witkowska, J.S. Suri, A review on ultrasound-based thyroid cancer tissue characterization and automated classification, Technol. Canc. Res. Treat. 13 (4) (2014) 289–301.
[10] L.N. Li, J.H. Ouyang, H.L. Chen, D.Y. Liu, A computer aided diagnosis system for thyroid disease using extreme learning machine, J. Med. Syst. 36 (5) (2012) 3327–3337.
[11] V.K. Sudarshan, M.R.K. Mookiah, U.R. Acharya, V. Chandran, F. Molinari, H. Fujita, K.H. Ng, Application of wavelet techniques for cancer diagnosis using ultrasound images: a review, Comput. Biol. Med. 69 (2016) 97–111.
[12] L. Ozyilmaz, T. Yildirim, Diagnosis of thyroid disease using artificial neural network methods, in: Proceedings of the 9th International Conference on in Neural Information Processing, 2002, pp. 2033–2036.
[13] K. Polat, S. Sahan, S. Gunes, A novel hybrid method based on artificial immune recognition system (airs) with fuzzy weighted pre-processing for thyroid disease diagnosis, Expert Syst. Appl. 32 (4) (2007) 1141–1147.
[14] M.A. Savelonas, D.K. Iakovidis, N. Dimitropoulos, D. Maroulis, Computational characterization of thyroid tissue in the radon domain, in: 20th IEEE International Symposium on Computer Based Medical Systems, 2007, pp. 189–192.
[15] A. Keles, A. Keles, ESTDD: expert system for thyroid diseases diagnosis, Expert Syst. Appl. 34 (1) (2008) 242–246.

[16] H. Kodaz, S. Ozsen, A. Arslan, S. Gunes, Medical application of information gain based artificial immune recognition system (airs): diagnosis of thyroid disease, Expert Syst. Appl. 36 (2) (2009) 3086–3092.
[17] E. Dogantekin, A. Dogantekin, D. Avci, An automatic diagnosis system based on thyroid gland: ADSTG, Expert Syst. Appl. 37 (9) (2010) 6368–6372.
[18] E. Dogantekin, A. Dogantekin, D. Avci, An expert system based on generalized discriminant analysis and wavelet support vector machine for diagnosis of thyroid diseases, Expert Syst. Appl. 38 (1) (2011) 146–150.
[19] H.L. Chen, B. Yang, G. Wang, J. Liu, Y.D. Chen, D.Y. Liu, A three-stage expert system based on support vector machines for thyroid disease diagnosis, J. Med. Syst. 36 (3) (2011) 1953–1963.
[20] D.Y. Liu, H.L. Chen, B. Yang, X.E. Lv, L.N. Li, J. Liu, Design of an enhanced fuzzy knearest neighbor classifier based computer aided diagnostic system for thyroid disease, J. Med. Syst. 36 (5) (2011) 3243–3254.
[21] A.T. Azar, S.A. El-Said, A.E. Hassanien, Fuzzy and hard clustering analysis for thyroid disease, Comput. Meth. Progr. Biomed. 111 (1) (2013) 1–16.
[22] U.R. Acharya, S.V. Sree, M.M.R. Krishnan, F. Molinari, R. Garberoglio, J.S. Suri, Non-invasive automated 3D thyroid lesion classification in ultrasound: a class of thyroscan systems, Ultrasonics 52 (4) (2012) 508–520.
[23] U.R. Acharya, O. Faust, S.V. Sree, F. Molinari, J.S. Suri, Thyroscreen system: high resolution ultrasound thyroid image characterization into benign and malignant classes using novel combination of texture and discrete wavelet transform, Comput. Meth. Progr. Biomed. 107 (2) (2012) 233–241.
[24] U.R. Acharya, S.V. Sree, M.R.K. Mookiah, R. Yantr, F. Molinari, W. Zieleźnik, J. Malyszek-Tumidajewicz, B. Stepien, R.H. Bardales, A. Witkowska, J.S. Suri, Diagnosis of hashimotos thyroiditis in ultrasound using tissue characterization and pixel classification, J. Eng. Med. 227 (7) (2013) 788–798.
[25] U.R. Acharya, S.V. Sree, M.R.K. Mookiah, F. Molinari, W. Zieleźnik, R.H. Bardales, A. Witkowska, J.S. Suri, Computer aided diagnostic system for detection of hashimoto thyroiditis on ultrasound images from a Polish population, J. Ultrasound Med. 33 (2) (2014) 245–253.
[26] U.R. Acharya, P. Chowriappa, H. Fujita, S. Bhat, S. Dua, J.E.W. Koh, L.W.J. Eugene, P. Kongmebhol, K.H. Ng, Thyroid lesion classification in 242 patient population using gabor transform features from high resolution ultrasound images, Knowl. Based Syst. 171 (2016) 235–245.
[27] Zbigniew Omiotek, Fractal analysis of the grey and binary images in diagnosis of Hashimoto's thyroiditis, Biocybern. Biomed. Eng. 37 (4) (2017) 655–665.
[28] Jianning Chi1, Ekta Walia, Paul Babyn, Jimmy Wang, Gary Groot, Mark Eramian, Thyroid nodule classification in ultrasound images by fine-tuning deep convolutional neural network, J. Digit. Imag. 30 (2017) 477–486.
[29] Priti S. Dhaygude, S.M. Handore, Detection of thyroid nodule in ultrasound images using artificial neural network, Int. J. Adv. Comput. Eng. Netw. 4 (2) (2016).
[30] H.M. Gireesha, S. Nanda, Thyroid nodule segmentation and classification in ultrasound images, Int. J. Eng. Res. Technol. 3 (5) (2014).
[31] Eung-HunKim SiLuo, YongminKim ManjiriDighe, Thyroid nodule classification using ultrasound elastography via linear discriminant analysis, Ultrasonics 51 (4) (May 2011) 425–431.
[32] Tianjiao Liu, Shuaining Xie, Yukang Zhang, Jing Yu, Lijuan Niu, Weidong Sun, Feature Selection And Thyroid Nodule, Classification using transfer learning, in: IEEE 14th International Symposium on Biomedical Imaging, ISBI, 2017.
[33] Deepika Koundal, Savita Gupta, Sukhwinder Singh, Computer-aided thyroid nodule detection system using medical ultrasound images, Biomed. Signal Process Contr. 40 (2018) 117–130.
[34] Lina Pedraza, Carlos Vargas, Fabián Narváez, Oscar Durán, Emma Muñoz, Eduardo Romero, An open access thyroid ultrasound-image Database, in: 10th International Symposium on Medical Information Processing and Analysis, 2015. SPIE 9287.
[35] N. Dalal, B. Triggs, Histograms of oriented gradients for human detection, in: Proc. IEEE Int. Conf. Comput. Vis. Pattern Recognit., USA, 2005, pp. 886–893.
[36] S.A.M. Al-Sumaidaee, M.A.M. Abdullah, R.R.O. Al-Nima, S.S. Dlay, J.A. Chambers, Multi-gradient features and elongated quinary pattern encoding for image-based facial expression recognition, Pattern Recogn. 71 (2017) 249–263.
[37] Y.C. Kim, E.J. Powers, Digital bispectral analysis and its applications to nonlinear wave interactions, IEEE Trans. Plasma Sci. 7 (1979) 120–131.
[38] G.B. Giannakis, Cumulants: a powerful tool in signal processing, Proc. IEEE 75 (1987) 1333–1334.
[39] V. Chandran, S. Elgar, Bispectral analysis of two-dimensional random processes, IEEE Trans. Acoust. Speech Signal Process. 38 (1990) 2181–2186.
[40] K.C. Chua, V. Chandran, U.R. Acharya, C.M. Lim, Cardiac state diagnosis using higher order spectra of heart rate variability, J. Med. Eng. Technol. 32 (2) (2008) 145–155.
[41] Anjan Gudigar, Shreesha Chokkadi, U. Raghavendra, U. Rajendra Acharya, Local texture patterns for traffic sign recognition using higher order spectra, Pattern Recogn. Lett. 94 (2017) 202–210.
[42] U.R. Acharya, R. Yanti, Jia Wei Zheng, M. Muthu Rama Krishnan, Jen Hong Tan, Roshan Joy Martis, Choo Min Lim, Automated diagnosis of epilepsy using Cwt, Hos and texture parameters, Int. J. Neural Syst. 23 (3) (2013), 1350009.
[43] Roshan Joy Martis, U. Rajendra Acharya, K.M. Mandana, A.K. Ray, Chandan Chakraborty, Cardiac Decision making using higher order spectra, Biomed. Signal Process Contr. 8 (2013) 193–203.
[44] U.R. Acharya, S.V. Sree, S. Chattopadhyay, J.S. Suri, Automated diagnosis of normal and alcoholic EEG signals, J. Neural Syst. 22 (03) (2012), 1250011.
[45] K.C. Chua, V. Chandran, U.R. Acharya, C.M. Lim, Automatic identification of epilepsy by HOS and power spectrum parameters using EEG signals: a comparative study, in: 30th Annual International IEEE EMBS Conference Vancouver, British Columbia, Canada, August 20-24, 2008.
[46] K.C. Chua, V. Chandran, U.R. Acharya, C.M. Lim, Higher order spectral (HOS) analysis of epileptic EEG signals, in: Proceedings of the 29th Annual International Conference of the IEEE EMBS, Cité Internationale, Lyon, France, August 23-26, 2007.
[47] Haibo He, Yang Bai, Edwardo A. Garcia, Shutao Li, ADASYN: adaptive synthetic sampling approach for imbalanced learning, in: 2008 IEEE International Joint Conference on Neural Networks, 2008, pp. 1322–1328. Hong Kong, China.
[48] J. Kennedy, R. Eberhart, Particle swarm optimization, in: Proceedings of the Sixth International Symposium on Micro Machine and Human Science, Nagoya, Japan, 1995, pp. 39–43.
[49] R. Batuwita, V. Palade, Class imbalance learning methods for support vector machines, in: Haibo He, Yunqian Ma Ma (Eds.), Imbalanced Learning: Foundations, Algorithms and Applications, Wiley, 2013.
[50] R. Akbani, S. Kwek, N. Japkowicz, Applying support vector machines to imbalanced datasets, in: Proceedings ECML, 2004, pp. 39–50.
[51] C.J.C. Burges, A Tutorial on Support Vector Machines for Pattern Recognition Data Min. Knowl. Discov., vol. 2, Kluwer Academic Publishers, 1998, pp. 121–167.
[52] M.A. Savelonas, D.K. Iakovidis, N. Dimitropoulos, D. Maroulis, Computational characterization of thyroid tissue in the radon domain, in: Proceedings of 12th IEEE International Symposium on Computer-based Medical Systems, Slovenia, 2007, pp. 189–192.
[53] S. Tsantis, N. Dimitropoulos, D. Cavouras, G. Nikiforidis, Morphological and wavelet features towards sonographic thyroid nodules evaluation, Comput. Med. Imag. Graph. 33 (2009) 91–99.
[54] J. Ma, S. Luo, M. Dighe, D. Lim, Y. Kim, Differential diagnosis of thyroid nodule with ultrasound elastography based on support vector machines, in: International Ultrasonics Symposium, 2010, pp. 1372–1375.
[55] C.Y. Chang, S.J. Chen, M.F. Tsai, Application of support-vector-machine-based method for feature selection and classification of thyroid nodules in ultrasound images, Pattern Recogn. 43 (2010) 3494–3506.
[56] D.K. Iakovidis, E.G. Keramidas, D. Maroulis, Fusion of fuzzy statistical distributions for classification of thyroid ultrasound patterns, Artif. Intell. Med. 50 (1) (2010) 33–41.
[57] J. Ding, H. Cheng, C. Ning, J. Huang, Y. Zhang, Quantitative measurement for thyroid cancer characterization based on elastography, J. Ultrasound Med. 30 (9) (2011) 1259–1266.
[58] I.N. Legakis, M. Savelonas, D.E. Maroulis, D. Iakovidis, Computer-based nodule malignancy risk assessment in thyroid ultrasound images, Int. J. Comput. Appl. 33 (1) (2011) 29–35.
[59] N. Singh, A. Jindal, Ultra sonogram images for thyroid segmentation and texture classification in diagnosis of malignant (cancerous) or benign (noncancerous) nodules, Int. J. Eng. Innovative Technol 1 (5) (2012) 202–206.
[60] E.G. Keramidas, D. Maroulis, D.K. Iakovidis, TND: a thyroid nodule detection system for analysis of ultrasound images and videos, J. Med. Syst. 36 (2012) 1271–1281.
[61] U. Raghavendra, U.R. Acharya, Anjan Gudigar, Jen Hong Tan, Hamido Fujita, Yuki Hagiwara, Filippo Molinari, Pailin Kongmebhol, Kwan Hoong Ng, Fusion of spatial gray level dependency and fractal texture features for the characterization of thyroid lesions, Ultrasonics 77 (2017) 110–120.